

Review

# Structure–Superstructure Inter-Relations in $\text{Ca}_2\text{SiO}_4$ Belite Phase

Vassilis Psycharis <sup>1,\*</sup>, Manolis Chatzigeorgiou <sup>1,2</sup>, Dimitra Koumpouri <sup>3</sup>, Margarita Beazi-Katsioti <sup>2</sup> and Marios Katsiotis <sup>4</sup>

<sup>1</sup> Institute of Nanoscience and Nanotechnology, National Center for Scientific Research “Demokritos”, 15310 Athens, Greece

<sup>2</sup> School of Chemical Engineering, National Technical University of Athens, 15772 Athens, Greece

<sup>3</sup> Independent Researcher, 15451 Athens, Greece

<sup>4</sup> Group Innovation & Technology, TITAN Cement S.A., 11143 Athens, Greece

\* Correspondence: v.psycharis@inn.demokritos.gr; Tel.: +30-210-6503346

**Abstract:** Belite, the second most abundant mineralogical phase in Portland cement, presents five polymorphs which are formed at different temperatures. The increased interest in belite cement-based products is due to the lower environmental impact associated with the lower energy consumption. The importance of belite polymorphs formed at higher temperatures for cement industry applications is high, because they present better hydraulic properties. Thus, any study that helps to explore the structure relations of all belite polymorphs is of interest for both scientific and practical points of view. In the present work, a systematic structure–superstructure relation study is presented for all polymorphs, and it is based on the work of O’Keefe and Hyde (1985). In this pioneering work, generally, the structures of oxides are considered as having common characteristics with prototype structures of alloys. The basic result of the present work is the fact that all the polymorphs adopt a common architecture which is based on capped trigonal prisms of Ca cations, which host the Si one, and the oxygen anions occupy interstitial sites, i.e., an architecture in conformity with the model which considers the oxide structures as stuffed alloys. This result supports the displacive character of the transformation structural mechanism that links the five polymorphs based on the cation sites in their structures. However, based on the sites of oxygen anions, it could be considered as of diffusion character. The study of belite polymorphs is also of interest to products obtained by doping dicalcium silicate compounds, which present interesting luminescent properties.

**Keywords:** belite; structure superstructure; stuffed alloys



**Citation:** Psycharis, V.; Chatzigeorgiou, M.; Koumpouri, D.; Beazi-Katsioti, M.; Katsiotis, M. Structure–Superstructure Inter-Relations in  $\text{Ca}_2\text{SiO}_4$  Belite Phase. *Crystals* **2022**, *12*, 1692. <https://doi.org/10.3390/cryst12121692>

Academic Editors: Sanja Burazer and Lidija Androš Dubraja

Received: 3 October 2022

Accepted: 17 November 2022

Published: 23 November 2022

**Publisher’s Note:** MDPI stays neutral with regard to jurisdictional claims in published maps and institutional affiliations.



**Copyright:** © 2022 by the authors. Licensee MDPI, Basel, Switzerland. This article is an open access article distributed under the terms and conditions of the Creative Commons Attribution (CC BY) license (<https://creativecommons.org/licenses/by/4.0/>).

## 1. Introduction

Alite (~50–70%) and belite (~20–30%) are the main mineralogical phases of Portland cement (OPC), accompanied by the presence of tricalcium aluminate and ferrite phases. Using the compact mineralogical code names, these four phases are represented by  $\text{C}_3\text{S}$  for  $\text{Ca}_3\text{SiO}_5$  (alite),  $\text{C}_2\text{S}$  for  $\text{Ca}_2\text{SiO}_4$  (belite),  $\text{C}_3\text{A}$  for  $\text{Ca}_3\text{Al}_2\text{O}_6$  or  $(\text{CaO})_3(\text{Al}_2\text{O}_3)$  (tricalcium aluminate), and  $\text{C}_4\text{AF}$  for  $\text{Ca}_4\text{Al}_2\text{Fe}_2\text{O}_{10}$  or  $(\text{CaO})_4(\text{Al}_2\text{O}_3)(\text{Fe}_2\text{O}_3)$ , where C = CaO, S =  $\text{SiO}_2$ , A =  $\text{Al}_2\text{O}_3$  and F =  $\text{Fe}_2\text{O}_3$  [1]. All the mineral phases of OPC cement are available in different polymorphic forms. The polymorphism of the mineral phases of cement depends on several parameters, such as the temperature and duration of heat treatment, cooling rate, the composition of the raw mixture and the presence of “stabilizer oxides” in the raw mixture. The formation of different polymorphic mineral phases in cement products is critical for their performance (hydraulic properties), as their presence directly affects the physical (fineness, setting time and volume stability) and mechanical (strength development) properties of cement.

For belite, tricalcium aluminate and ferrite phases, the structures of their different polymorphs are well studied and known, i.e.,  $\text{C}_2\text{S}$  [2–4],  $\text{C}_3\text{A}$  [5,6] and  $\text{C}_4\text{AF}$  [7,8]. Alite

and belite present many polymorphs. Their structure–superstructure relations are used to explore the structural connection among them and also to understand the mechanism governing the transformation from one polymorph to the other [9,10]. In a series of papers [9,11–14], a thorough analysis of the structure–superstructure relations for alite is given. In the framework of this analysis [13], new structural models for alite polymorphs have been proposed and are used in the analysis of powder diffraction diagrams with the Rietveld method of industrial cement products.

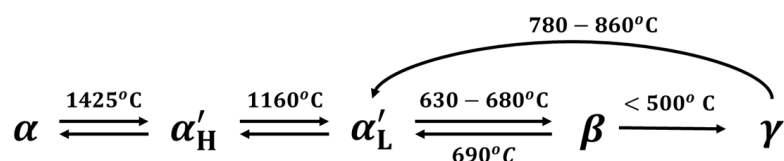
The increased interest in the use of belite-based cement products is due to the need for lower energy consumption and their positive environmental impact compared to OPC [15]. The recent increased research interest and study of luminescent belite-based doped compounds [16] make the understanding of belite polymorph formation and stabilization very attractive and the need for accurate belite polymorphism identification essential. The belite phase presents five polymorphs, and these are listed below based on the decreasing formation temperature, i.e.,  $\alpha$ -Ca<sub>2</sub>SiO<sub>4</sub> ( $\alpha$ -C<sub>2</sub>S, 1545 °C),  $\alpha'$ <sub>H</sub>-Ca<sub>2</sub>SiO<sub>4</sub> ( $\alpha'$ <sub>H</sub>-C<sub>2</sub>S, 1250 °C),  $\alpha'$ <sub>L</sub>-Ca<sub>2</sub>SiO<sub>4</sub> ( $\alpha'$ <sub>L</sub>-C<sub>2</sub>S, 1060 °C),  $\beta$ -Ca<sub>2</sub>SiO<sub>4</sub> ( $\beta$ -C<sub>2</sub>S, <500 °C) and  $\gamma$ -Ca<sub>2</sub>SiO<sub>4</sub> ( $\gamma$ -C<sub>2</sub>S, stable at room temperature). The “activity” (better hydraulic properties) of the belite polymorphs is higher at high formation temperatures (belite polymorph activity:  $\alpha > \alpha'_H > \alpha'_L > \beta$ ) [1,17], while  $\gamma$ -C<sub>2</sub>S does not exhibit hydraulic properties.  $\beta$ -C<sub>2</sub>S is the high-temperature monoclinic polymorph of the Calcio-Olivine  $\gamma$ -C<sub>2</sub>S polymorph but does not belong to the olivine group. The structure relations of the family of belite polymorphs are discussed in detail in [10]. It is well known that the first four of them,  $\alpha$ -,  $\alpha'_H$ -,  $\alpha'_L$ - and  $\beta$ -C<sub>2</sub>S, are inter-related with reversible phase transitions [4,18–20]. The structural basis for these transformations is explained by their similarity to the structure of K, Na-glaserite sulfate, K<sub>3</sub>Na[SO<sub>4</sub>]<sub>2</sub> and its derivative  $\beta$ -K<sub>2</sub>[SO<sub>4</sub>] Arcanite ( $\alpha'_H$ -,  $\alpha'_L$ - and  $\beta$ -C<sub>2</sub>S) [10]. The main result of these studies is the coordination polyhedra formed by oxygen atoms around the cations, and the framework build by the polyhedra arrangement within the structures of these polymorphic phases. The relation of the framework formed by the coordination polyhedra in the structure of glaserite and that of  $\beta$ -C<sub>2</sub>S is also discussed in [21].

The description of structures based on polyhedra of anions is the traditional point of view introduced by Pauling [22] and is based on the idea that the “small” cations occupy positions in the voids left in their crystal structure by the larger atoms of anions such as oxygens [23,24]. A new approach has been introduced by O’Keefe and Hyde [23], where the role of ions is reversed, i.e., the structure description is based on the packing of cations and the anions are inserted at interstitial sites among them. In the beginning, this new approach was considered purely geometric, and no bonding type considerations were implied for the atoms involved in the packing within a crystal structure. However, recently, in addition to the achieved simplifications in the presentation of many structures, the role of cations was reconsidered as the packing of cations observed within the ionic structures resamples those observed in their parent metal structures [25]. The geometric characteristics, arrangement and distances in the parent alloy structures are retained in the ionic one [24]. More interestingly, based on the pioneering work in this field by O’Keefe and Hyde [23], it is found that in ternary oxides with two different metals the packing of cations corresponds to the packing of the binary alloys of the metals. Therefore, in the case of  $\beta$ -C<sub>2</sub>S, the cations’ packing resembles that of Ni<sub>2</sub>In prototype structure (B8<sub>b</sub>, Strukturbericht designations). These observations have made the authors O’Keefe and Hyde characterize the oxides as “stuffed alloys”. With a lack of data from the other belite polymorphs, the discussion by Barbier and Hyde (1985) [26] using the cation-stuffed model of oxides is restricted on the structure inter-relations of  $\beta$ - and  $\gamma$ -Ca<sub>2</sub>SiO<sub>4</sub> dicalcium silicates. In addition, they extended their study to  $\alpha'$ - and  $\beta$ -Sr<sub>2</sub>SiO<sub>4</sub> polymorphs which resemble the structures of the corresponding polymorphs of belite. The ideas developed in the works of Barbier and Hyde [26] and O’Keefe and Hyde [23] are applied systematically in the present work for the study of all polymorphs of belite. This analysis of all the belite polymorphic structures, which is based on the observation of common building blocks of

prototype alloy structures, revealed first the geometric basis of the structure–superstructure inter-relations and second possible transformation mechanisms.

## 2. Methodology

In this section, the methodology of the present study is developed, which essentially consists at a first step of the description of the arrangement of cations in prototype alloy structures and their relation to the structures of  $\beta$ -C<sub>2</sub>S and  $\gamma$ -C<sub>2</sub>S belite polymorphs, as have been discussed in previous studies [23,26]. Then, in the next section this discussion is extended to the other polymorphs as well. According to Mumme [4], the Ca<sub>2</sub>SiO<sub>4</sub> compound presents five polymorphs (Scheme 1):



**Scheme 1.** Belite polymorphs formed at different temperatures.

The decreasing order of formation/stabilization temperature of the belite polymorphs is  $\alpha$ -,  $\alpha'_{\text{H}}$ -,  $\alpha'_{\text{L}}$ -,  $\beta$ - and  $\gamma$ -C<sub>2</sub>S.  $\beta$ -C<sub>2</sub>S is metastable and can be formed during cooling but cannot be produced from  $\gamma$ -C<sub>2</sub>S on heating. Unless  $\beta$ -C<sub>2</sub>S is stabilized during cooling, the  $\alpha$ - and  $\alpha'$ -C<sub>2</sub>S polymorphs revert to the stable form of  $\gamma$ -C<sub>2</sub>S. The subscript H stands for the high- and L for the low-temperature form of  $\alpha'$  polymorphs. Stabilization of the “active” belite polymorphs and also prevention of the transition from  $\beta$  to  $\gamma$ -C<sub>2</sub>S can be achieved by rapid cooling and/or by incorporation of a “stabilizer” (substitution of Ca and Si cations by cations of Ti, B, S, K, etc.) in the belite structure [19,20,27–29].

In their original articles, Barbier and Hyde [26] and O’Keefe and Hyde [23] use two prototype metal alloy structures to describe  $\beta$ -C<sub>2</sub>S and  $\gamma$ -C<sub>2</sub>S belite polymorphs. These are the prototype structure of PbCl<sub>2</sub> (Strukturbericht designations C23) and Ni<sub>2</sub>In (B8<sub>b</sub> type), respectively. The  $\beta$ -C<sub>2</sub>S polymorph is also compared to the Ca<sub>2</sub>Si alloy, which is similarly characterized by the C23 Strukturbericht structure type. The  $\beta$ - and  $\gamma$ -C<sub>2</sub>S polymorphs are also discussed in comparison to the structures of low- and high-temperature K<sub>2</sub>SO<sub>4</sub> compounds, which belong to the Strukturbericht C23 and B8<sub>b</sub> types of compounds, respectively.

In Table 1, we provide general information and ICSD codes for all the compounds that are discussed in the present work. Detailed crystallographic data for the structures of all the polymorphs and prototype phases are provided in Table S2, together with all references from where all the data were obtained. In the present work, a systematic structural study of all the polymorphs of belite and their inter-relations is attempted using the approach of O’Keefe and Hyde. To ensure that the structural models were obtained by analyzing data from materials synthesized in similar ways, we decided to use the models given in reference Mumme (1995) [3] for  $\beta$ -C<sub>2</sub>S and Mumme (1996) [4] for the rest of belite polymorphs. Details for the structures of all polymorphs are given in Table S2. Plots of the structures were drawn using the Diamond-3.1 program package [30].

The prototype structure of Ni<sub>2</sub>In (B8<sub>b</sub>) crystallizes in the *P*6<sub>3</sub>/*mmc* Space Group (S.G.) [31]. Atoms in the unit cell are arranged as in Figure 1A. Following the original description [23], Ni atoms are packed in trigonal Ni<sub>6</sub> prisms that host the In atoms and, by sharing their trigonal faces, form columns parallel to the direction [110]. The trigonal prisms, as they are the basic polyhedra that characterize the structures studied in this work, are demarcated by orange lines in all the pictures. These columns are arranged in a zig-zag fashion above and below (1–100) planes, and by edge-sharing they form “walls” parallel to these planes. In Figure 1B, the arrangement of atoms is shown in projection on the (11–20) planes, and in Figure 1C the same view is shown tilted to make clear the relative arrangement of crystallographic planes. It is mentioned that the atoms on the “wall” in the middle of Figure 1B,C, those indicated with the yellow arrows, are shifted along the direction normal to the (11–20) planes by a distance half the height of the trigonal

prisms, which is equal to the  $d_{11-20}$  plane distance. For the description of all the structures discussed in the present work on a common basis, it is useful to use in addition to the hexagonal cell the ortho-hexagonal one [32]. The relative orientation of ortho-hexagonal cell axes is shown in Figure 1B and their relation with the hexagonal axes in Figure 2D.

**Table 1.** Structural information and parameters for the prototype 8B2 and C23 prototype structures and the five polymorphs of belite ( $\text{Ca}_2\text{SiO}_4$ ).

Phase Code Name	ICSD #	Space Group	V/Z
8B <sub>b</sub> (InNi <sub>2</sub> )	640098 [31]	$P6_3/mmc$	-
C23 (Ca <sub>2</sub> Si)	158275 [32]	$Pnma$	-
$\alpha_{\text{H}}$ -C <sub>2</sub> S	82998 [4]	$P6_3/mmc$	97.10 Å <sup>3</sup>
$\alpha_{\text{Tr}}$ -C <sub>2</sub> S	82999 [4]	$P-3m1$	97.10 Å <sup>3</sup>
$\alpha'_{\text{H}}$ -C <sub>2</sub> S	82997 [4]	$Pnma$	91.94 Å <sup>3</sup>
$\alpha'_{\text{L}}$ -C <sub>2</sub> S	82996 [4]	$Pna2_1$	90.79 Å <sup>3</sup>
$\beta$ -C <sub>2</sub> S	81096 [3]	$P2_1/n$	86.45 Å <sup>3</sup>
$\gamma$ -C <sub>2</sub> S	82994 [4]	$Pbnm$	96.18 Å <sup>3</sup>

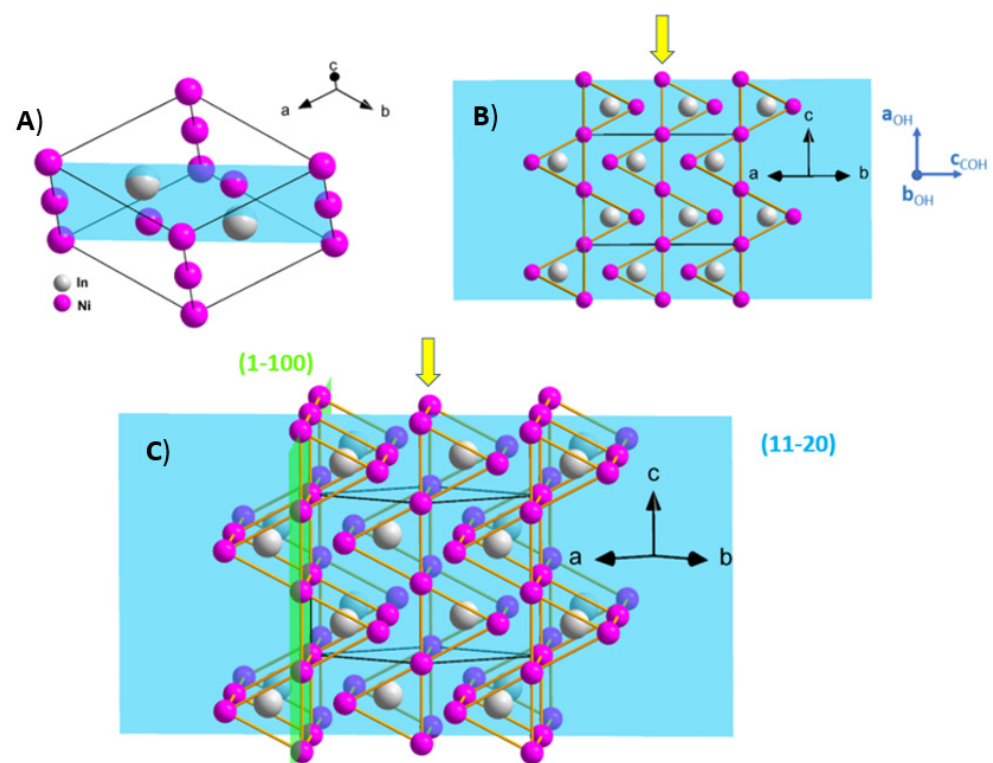


**Figure 1.** (A) Arrangement of atoms in the cell of the Ni<sub>2</sub>In structure. (B) “Walls” of trigonal prisms parallel to the (1–100) planes projected on the (11–20) planes. The relative orientation of the ortho-hexagonal reference system is also indicated. The former plane is normal, and the second one is parallel to the plane of the figure and (C) tilted view. The planes (11–20) and (1–100) are shown in cyan and light green color, respectively. The orange lines are delimitating the trigonal prisms. The yellow arrows indicate the middle “wall” arrangement of trigonal prisms and the reference system, with axes drawn in blue indicating the orientation of the ortho-hexagonal axes system.

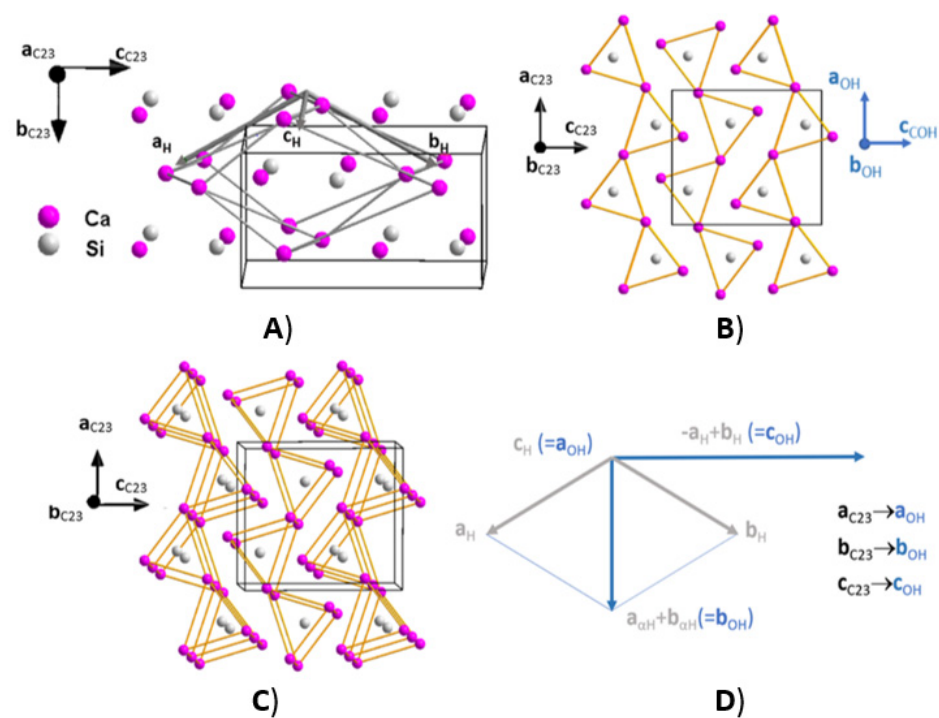


**Figure 2.** (A) Arrangement of atoms in the cell of the  $\text{Ca}_2\text{Si}$  structure cell. Light grey lines joining Ca cations indicate the orientation of the hexagonal part of the structure within the prototype structure C23. With dark grey vectors the orientation of the reference hexagonal cell is also shown. (B) “Walls” of trigonal prisms parallel to the planes (001) projected on the (010) planes. The former planes are normal, and the latter ones are parallel to the plane of the figure. The relative orientation of the ortho-hexagonal reference system is also indicated. (C) Presents a tilted view of (B). (D) Schematic presentation of the unit cell axes relations for the hexagonal and ortho-hexagonal cells. The correspondences of the cell axes of the orthorhombic C23 type structure with those of ortho-hexagonal cell are also indicated.

The arrangement of atoms in the  $\text{Ca}_2\text{Si}$  alloy, which crystallizes in the  $Pnma$  S.G. [32], with the C23 Strukturbericht structure type, is shown in Figure 2. The atoms in the structure of the  $\text{Ca}_2\text{Si}$  alloy are packed again in trigonal  $\text{Ca}_6$  prisms which host the Si atoms and by sharing their trigonal faces form columns parallel to the  $b$  crystallographic axis. These columns are arranged in a zig-zag fashion above and below the (001) planes, and by edge-sharing they form “walls” parallel to these planes. In Figure 2B, the arrangement of atoms is shown in projection on (010) planes, and in Figure 2C the same view is shown tilted. It is mentioned that also in the present case, the atoms on the “wall” in the middle of Figure 2B,C are shifted along the  $a$ -axis direction by a distance half the high of the trigonal prisms, which is equal to the  $d_{100}$  plane distance. The main difference in the present arrangement from the one presented in Figure 1A,C is that in the second case the “walls” are puckered. In Figure 2A, in addition to atom arrangement within the unit cell the relative position of the hexagonal axes system is shown, which helps to derive the relationship which joins the hexagonal with the orthorhombic cell. The relative orientation of the cell axes of the two systems is shown in Figure 2D. The relative orientation of the ortho-hexagonal cell axes with those of the orthogonal ones is also indicated (Figure 2B,D), and they are identical. Thus, there is a one-to-one correspondence among  $a_{\text{C23}}$ ,  $b_{\text{C23}}$  and  $c_{\text{C23}}$  and  $a_{\text{OH}}$ ,  $b_{\text{OH}}$  and  $c_{\text{OH}}$  axes, respectively, which is expressed with the relations  $a_{\text{C23}} \rightarrow a_{\text{OH}} = c_{\text{H}}$ ,  $b_{\text{C23}} \rightarrow b_{\text{OH}} = a_{\text{H}} + b_{\text{H}}$  and  $c_{\text{C23}} \rightarrow c_{\text{OH}} = -a_{\text{H}} + b_{\text{H}}$ , where the C23, OH and H subscripts stand for orthorhombic, ortho-hexagonal and hexagonal cells, respectively. The prototype structures of  $\text{Ni}_2\text{In}$  and  $\text{Ca}_2\text{Si}$ , which are discussed in the present section, are used as a basis to describe the structure inter-relation for all belite polymorphs. It worth to

notice that the  $c_{OH}$ -axis is normal to the planes of the “walls” and the  $a_{OH}$  and  $b_{OH}$  axes lie within these planes.

The transformation of  $\beta$ - $C_2S$  to  $\gamma$ - $C_2S$  has been discussed as a transformation of the C23 to B8b prototype arrangement of the Ca and Si cations [23,26]. The relative arrangements of  $Ca^{+2}$  cations and  $SiO_4^{-4}$  anions in the structures of these two polymorphs of belite are shown in Figures 3 and 4, respectively. Ca and Si atoms in the  $\beta$ - $C_2S$  polymorph of belite occupy the corresponding Ca and Si sites of the  $Ca_2Si$  (C23) prototype structure. In the  $\gamma$ - $C_2S$  polymorph, Ca and Si atoms occupy the sites of Ni and In atoms in the  $Ni_2In$  B8b prototype structure, respectively. The oxygen atoms in both cases are inserted at interstitial sites (Figures 3 and 4). In reference [23], the  $\beta$ - $C_2S$  to  $\gamma$ - $C_2S$  transformation is discussed in relation to the observed 11.2% of unit cell volume increase when the transformation takes place. This is also mentioned in reference [33], where ternary alloys undergo a C23 to B8b type structural transformation. The same transformation is also discussed on the basis of unit cell axes changes in both works. In Table 2, the unit cell axes relations for all studied structures with those of the ortho-hexagonal system are given, and through these relations all the structure inter-relations and changes are discussed. For ternary alloys, the transformation of 8Bb to C23 results in changes within the **a**, **b** planes, i.e., within the (001) “wall” planes of the ortho-hexagonal cell [33]. In references [26,34], the emphasis is given to the presentation of changes that take place at a local level and more specifically to the atomic displacements of the atoms that contribute to the formation of trigonal prisms and their surroundings. An attempt has been made in the past to extend the description based on the cation-staffed model of oxides to other belite polymorphs, using standard alloy structures, but so far, the discussion has been limited either to data from analogous structures [26] or to the interpretation of results from TEM studies [35]. The availability of structural data for all belite polymorphs [3,4] is exploited in the next section of the present work for the examination of all the structures of the corresponding polymorphs with the O’Keefe and Hyde model.

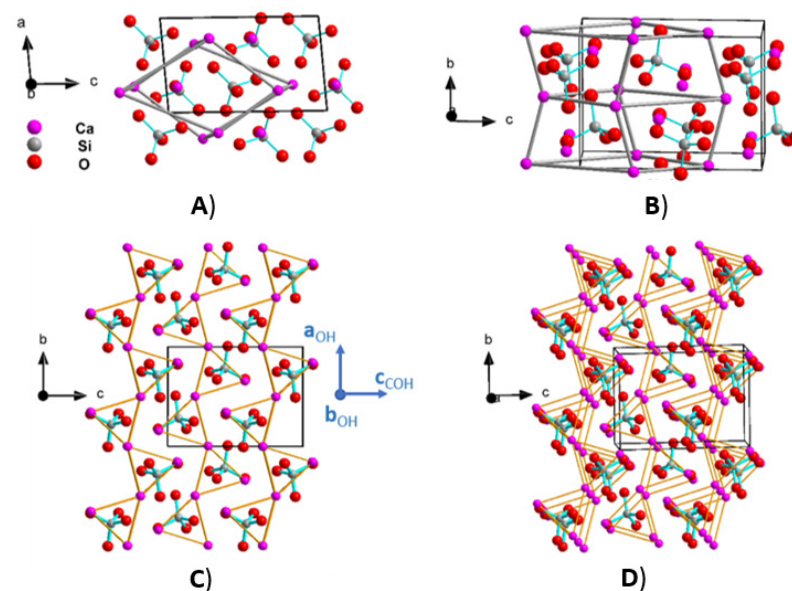


**Figure 3.** (A) The unit cell content of  $\beta$ - $Ca_2SiO_4$  polymorph viewed along the  $b$ -axis. Light grey lines joining Ca cations indicate the orientation of the hexagonal part of the structure and (B) side view of unit cell content along the  $a$ -axis is shown. (C) View along  $a$ -axis and the packing arrangement of trigonal prisms is demarcated with orange lines. The relative orientation of the ortho-hexagonal reference system is also indicated. (D) A tilted view of (C). The Si-O bonds are indicated by cyan lines.

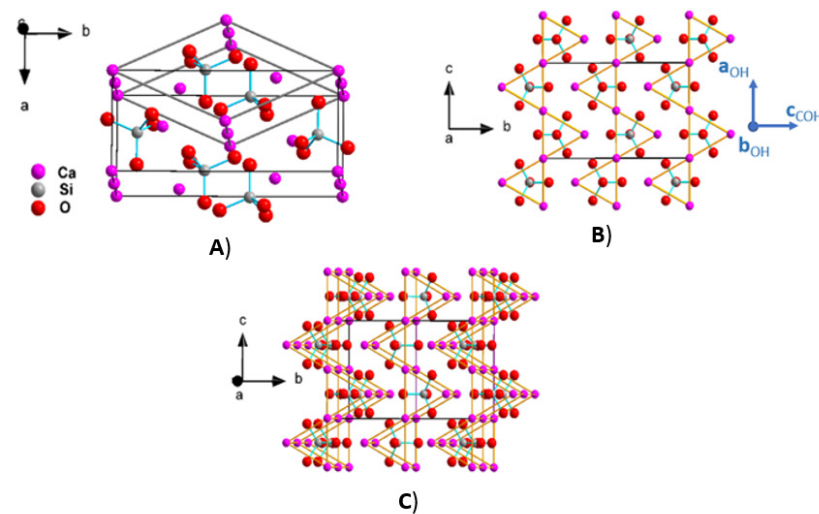


**Figure 4.** (A) The unit cell content of  $\gamma$ - $\text{Ca}_2\text{SiO}_4$  polymorph viewed along c-axis. Light grey lines joining Ca cations indicate the orientation of the hexagonal part of the structure. (B) View along the a-axis and the packing arrangement of trigonal prisms is demarcated with orange lines. The relative orientation of the ortho-hexagonal reference system is also indicated. (C) Tilted view of (B). The Si-O bonds are indicated by cyan lines.

**Table 2.** Unit cell relation of the C23 prototype structure and the unit cells of the five polymorphs of belite with the basic hexagonal unit cell of the 8B2 structure.

Phase Code Name	Unit Cell Axes	Cell Volume Relations
8B <sub>b</sub> (InNi <sub>2</sub> )	$\mathbf{a}_H, \mathbf{b}_H$ and $\mathbf{c}_H$	$V_H$
C23( $\text{Ca}_2\text{Si}$ )	$\mathbf{a}_{c23} = \mathbf{c}_H, \mathbf{b}_{c23} = \mathbf{a}_H + \mathbf{b}_H$ and $\mathbf{c}_{c23} = -\mathbf{a}_H + \mathbf{b}_H$	$2 \times V_H$
$\alpha_H$ -C <sub>2</sub> S	$\mathbf{a}_{\alpha H} \rightarrow \mathbf{a}_H, \mathbf{b}_{\alpha H} \rightarrow \mathbf{b}_H$ and $\mathbf{c}_{\alpha H} \rightarrow \mathbf{c}_H$ $a_{\alpha H} = 5.532 \text{ \AA}, b_{\alpha H} = 5.532$ and $c_{\alpha H} = 7.327$	$V_{\alpha H} \rightarrow V_H$
$\alpha_{Tr}$ -C <sub>2</sub> S	$\mathbf{a}_{\alpha Tr} = \mathbf{a}_{\alpha H}, \mathbf{b}_{\alpha Tr} = \mathbf{b}_{\alpha H}$ and $\mathbf{c}_{\alpha Tr} = \mathbf{c}_{\alpha H}$	$V_{\alpha Tr} = V_{\alpha H}$
$\alpha'_H$ -C <sub>2</sub> S	$\mathbf{a}_{\alpha' H} = \mathbf{c}_{\alpha H} (\rightarrow \mathbf{a}_{oH}), \mathbf{b}_{\alpha' H} = \mathbf{a}_{\alpha H} + \mathbf{b}_{\alpha H} (\rightarrow \mathbf{b}_{oH})$ and $\mathbf{c}_{\alpha' H} = -\mathbf{a}_{\alpha H} + \mathbf{b}_{\alpha H} (\rightarrow \mathbf{c}_{oH})$ $a_{\alpha' H} = 6.871 \text{ \AA} \rightarrow a_{oH} = 7.327 \text{ \AA}, b_{\alpha' H} = 5.601 \text{ \AA} \rightarrow b_{oH} = 5.532 \text{ \AA}$ and $c_{\alpha' H} = 9.556 \text{ \AA} \rightarrow c_{oH} = 9.581 \text{ \AA}$	$2 \times V_{\alpha H}$
$\alpha'_L$ -C <sub>2</sub> S	$\mathbf{a}_{\alpha' L} = 3\mathbf{c}_{\alpha H} (\rightarrow 3\mathbf{a}_{oH}), \mathbf{b}_{\alpha' L} = -\mathbf{a}_{\alpha H} + \mathbf{b}_{\alpha H} (\rightarrow \mathbf{c}_{oH}), \mathbf{c}_{\alpha' L} = -\mathbf{a}_{\alpha H} - \mathbf{b}_{\alpha H} (\rightarrow -\mathbf{b}_{oH})$ $a_{\alpha' L} = 20.527 \text{ \AA} \rightarrow 3a_{oH} = 21.981 \text{ \AA}, b_{\alpha' L} = 9.496 \text{ \AA} \rightarrow c_{oH} = 9.581 \text{ \AA}$ and $c_{\alpha' L} = 5.590 \text{ \AA} \rightarrow b_{oH} = 5.532 \text{ \AA}$	$6 \times V_{\alpha H}$
$\beta$ -C <sub>2</sub> S	$\mathbf{a}_\beta = -\mathbf{a}_{\alpha H} - \mathbf{b}_{\alpha H} (\rightarrow -\mathbf{b}_{oH}), \mathbf{b}_\beta = \mathbf{c}_{\alpha H} (\rightarrow \mathbf{a}_{oH}), \mathbf{c}_\beta = -\mathbf{a}_{\alpha H} + \mathbf{b}_{\alpha H} (\rightarrow \mathbf{c}_{oH})$ $a_\beta = 5.512 \text{ \AA} \rightarrow (b_{oH}) = 5.532 \text{ \AA}, b_\beta = 6.758 \text{ \AA} \rightarrow a_{oH} = 7.327 \text{ \AA},$ $c_{\beta \sin \beta} = 9.284 \text{ \AA} \rightarrow c_{oH} = 9.581 \text{ \AA}$ and $(\beta_\beta = 94.581^\circ \rightarrow \alpha_{oH} = 90.0^\circ)$	$2 \times V_{\alpha H}$
$\gamma$ -C <sub>2</sub> S	$\mathbf{a}_\gamma = \mathbf{a}_{\alpha H} + \mathbf{b}_{\alpha H} (\rightarrow \mathbf{b}_{oH}), \mathbf{b}_\gamma = -\mathbf{a}_{\alpha H} + \mathbf{b}_{\alpha H} (\rightarrow \mathbf{c}_{oH})$ and $\mathbf{c}_\gamma = \mathbf{c}_H (\rightarrow \mathbf{a}_{oH})$ $a_\gamma = 5.076 \text{ \AA} \rightarrow b_{oH} = 5.532 \text{ \AA}, b_\gamma = 11.214 \text{ \AA} \rightarrow c_{oH} = 9.581 \text{ \AA}$ and $c_\gamma = 6.758 \text{ \AA} \rightarrow a_{oH} = 7.327 \text{ \AA}$	$2 \times V_{\alpha H}$

### 3. Structure Inter-Relations for Belite Polymorphs

In this section, the structure inter-relation of all belite polymorphs are studied based on common patterns of the arrangement of cations using ideas which have been introduced previously. In Figure 5, the two models for  $\alpha$ -C<sub>2</sub>S, the high-temperature polymorph of belite, are presented, which have been proposed by Mumme [4]. The difference between the proposed models, a trigonal and a hexagonal one, concerns the arrangements of oxygen atoms of the SiO<sub>4</sub> tetrahedra, but in both models, the arrangement of Ca and Si cations resembles that of the B8b prototype structure, and these are shown in Figures 5B and 5D, respectively. The Rietveld refinement has promoted the hexagonal model for the  $\alpha$ -C<sub>2</sub>S polymorph [4], and this is the reason why the hexagonal cell axes are used to express these relations. As has been already mentioned above, the best way to track the changes which

are observed in this family of compounds is by using the ortho-hexagonal reference system which is derived from the hexagonal cell of the  $\alpha$ -C<sub>2</sub>S polymorph. The relative orientation of the ortho-hexagonal cell axes with respect to those of the reference hexagonal cell is shown in Figure 5B,D for the  $\alpha$ -C<sub>2</sub>S polymorph. In the first model, where the structure is described in a trigonal S.G. (Table 1), deviation of one oxygen atom from the c-axis is observed (Figure 5A). In the second model, where the structure is described in a hexagonal S.G. (Table 1), the oxygen atoms show severe disorder, and half of the SiO<sub>4</sub> tetrahedra point in one direction and half of them in the opposite one (Figure 5C). In Figure 6A,C, the unit cell content for the  $\alpha'$ <sub>H</sub>- and  $\alpha'$ <sub>L</sub>-C<sub>2</sub>S polymorphs are shown. In the same figure, their projection along the b-axis for the former (Figure 6B) and also along the c-axis for the latter (Figure 6D) are shown, revealing the resemblance to the C23 prototype structure for both polymorphs. The relative orientation of the ortho-hexagonal reference system with the crystal systems of  $\alpha'$ <sub>H</sub>-Ca<sub>2</sub>SiO<sub>4</sub> and  $\alpha'$ <sub>L</sub>-Ca<sub>2</sub>SiO<sub>4</sub> polymorphs is also indicated in Figure 6B,C, respectively. Concerning the SiO<sub>4</sub> tetrahedra, in the case of the  $\alpha'$ <sub>H</sub> polymorph, all oxygen atoms are disordered, in contrast to the  $\alpha'$ <sub>L</sub> where all the oxygens are ordered (Figure 6). In Figure 6A,B, the gray lines that join calcium atoms outline the part of the structure that corresponds to the basic hexagonal cell. A direct comparison of Figure 5A,B (or Figure 5C,D) with Figure 1A (or Figure 1B) makes clear that the arrangement of cations in the  $\alpha$ -C<sub>2</sub>S polymorph of belite resembles that in the Ni<sub>2</sub>In 8B<sub>b</sub> prototype, irrespective of the S.G. used for the structure description of this polymorph. Thus, for the study of the structure inter-relations of belite polymorphs, the structure of the  $\alpha$ -C<sub>2</sub>S polymorph is used for the rest of the text, as a prototype structure. The inter-relation of all the polymorphs of belite is concluded from the relation of the unit cell axes of each polymorph with the hexagonal cell axes of the  $\alpha$ -C<sub>2</sub>S polymorph and more specifically through their relation with the ortho-hexagonal ones. In Table 2, the inter-relation of the cells for the C23 and 8B<sub>b</sub> prototype structures are also listed, and their relation is presented schematically in Figure 2D. The relation among the structures of these two prototype structures is concluded on the fact that there is a one-to-one correspondence of the structures at an atomic level. This relation extends also to the reference systems of both structures, as there is also a one-to-one correspondence of the axes of the C23 structure with those of the ortho-hexagonal cell axes deduced from the hexagonal cell of the 8B<sub>b</sub> structure (Figure 2D). These relations are deduced concerning Figures 1A and 2A for the prototype C23 and 8B<sub>b</sub> structures. From the previous discussion and the presentations given so far for all the structures, and more specifically for those of belite polymorphs, it is clear that the arrangements of Ca and Si cations resemble that of the prototype structures, and the ortho-hexagonal reference system of the axes of the  $\alpha$ -C<sub>2</sub>S polymorph could be used for the expression of the structure inter-relations. The relations given in Table 2 for the unit cell axes of the polymorphs  $\alpha$ -C<sub>2</sub>S,  $\alpha'$ <sub>H</sub>-C<sub>2</sub>S,  $\alpha'$ <sub>L</sub>-C<sub>2</sub>S,  $\beta$ -C<sub>2</sub>S and  $\gamma$ -C<sub>2</sub>S with those of ortho-hexagonal ones were derived based on Figure 5D (or Figure 5B), Figure 6B,D, Figures 3C and 4B, respectively. In Table 2, in addition to the vector relations of the cell axes the values of the corresponding axes are given in order to facilitate their comparisons. In Figure 7A, the vector relations for all belite polymorphs with the ortho-hexagonal cell derived from the hexagonal cell of the  $\alpha$ -C<sub>2</sub>S polymorph are schematically presented. In Figure 7B, a diagram for the variation in the unit cell values is given for all the polymorphs as compared to the values of the ortho-hexagonal cell. Based on the variation in the cell values given in Figure 7B and Table 2, during the transformation of  $\alpha$ -C<sub>2</sub>S (8B<sub>b</sub>)  $\rightarrow$   $\alpha'$ <sub>H</sub>-C<sub>2</sub>S (C23) the variation in the cell axes concerns the  $a_{\alpha'H}$ ,  $b_{\alpha'H}$  axes ( $a, b$  ortho-hexagonal plane) with  $c_{\alpha'H}$  remaining almost constant in agreement with the corresponding variation observed for 8B<sub>b</sub>  $\rightarrow$  C23 transformation for ternary alloys [33]. For the rest of the polymorphs which have the C23 prototype structures ( $\alpha'$ <sub>L</sub>-C<sub>2</sub>S and  $\beta$ -C<sub>2</sub>S), a slight decrease is observed for all axes. The highest one is related to the equivalent to the  $c_{0H}$ ,  $c_{\beta}$ -axis of the beta polymorph. With the transformation  $\beta$ -C<sub>2</sub>S (C23)  $\rightarrow$   $\gamma$ -C<sub>2</sub>S (8B<sub>b</sub>), the  $c_{\gamma}$  (equivalent to  $a_{\alpha'H}$ -axis) value remains constant ( $b_{\beta} = 6.758 \text{ \AA} \rightarrow c_{\gamma} = 6.758 \text{ \AA}$ ) and the  $a_{\gamma}$  value (equivalent to  $b_{\alpha'H}$ -axis) is reduced ( $a_{\beta} = 5.512 \text{ \AA} \rightarrow a_{\gamma} = 5.076 \text{ \AA}$ ) but the  $b_{\gamma}$  value (equivalent to  $c_{\alpha'H}$ -axis) increases

significantly ( $c_{\beta \sin \beta} = 9.284 \text{ \AA} \rightarrow b_{\gamma} = 11.214 \text{ \AA}$ ). It is worth noticing that this axis is normal in the planes of “walls” of trigonal prisms. In all the studies of  $\beta\text{-C}_2\text{S}$  (C23)  $\rightarrow \gamma\text{-C}_2\text{S}$  (8Bb) transformation [23,26,33,35], the high increase in the volume of the cells of the corresponding cells is mentioned. In the study [35], which concerns ternary alloys, this variation is expressed by reference to the  $V_{\text{cell}}/Z$  (cell volume per formula unit) parameter. By using this value (last column of Table 1), this parameter starts from the value  $97.10 \text{ \AA}^3$  for the  $\alpha_{\text{H}}\text{-C}_2\text{S}$  polymorph then decreases to the value of  $86.45 \text{ \AA}^3$  for the  $\beta\text{-C}_2\text{S}$  polymorph and then increases again to the value of  $96.18 \text{ \AA}^3$  for the  $\gamma\text{-C}_2\text{S}$  polymorph.

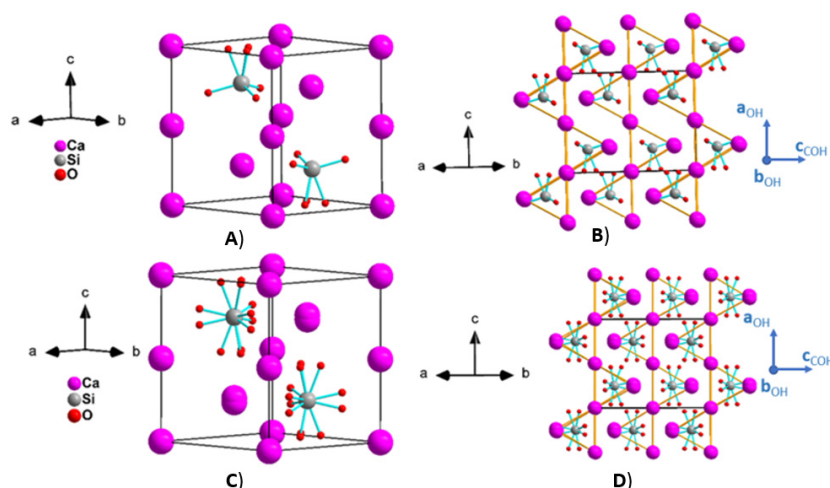


**Figure 5.** (A) The unit cell content and (B) the packing arrangement of trigonal prisms for the  $\alpha_{\text{T}}\text{-Ca}_2\text{SiO}_4$  polymorph structural model is shown. (C) The unit cell content and (D) the packing arrangement of the trigonal prisms for the  $\alpha_{\text{H}}\text{-Ca}_2\text{SiO}_4$  polymorph structural model are shown. Si-O bonds are indicated with cyan lines. In (B,D), the structures are projected on the (11–20) planes, the trigonal prisms are demarcated with orange lines and the relative orientation of the ortho-hexagonal reference system is also indicated.

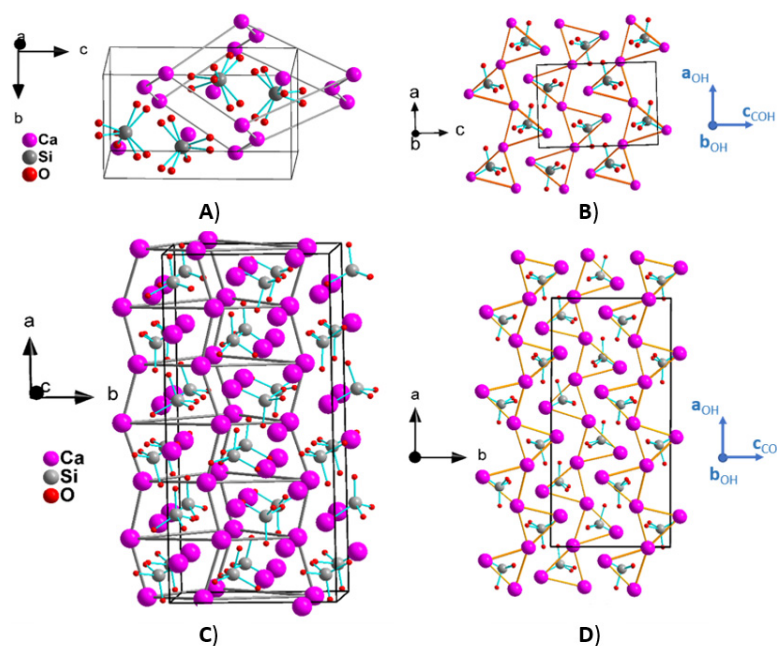


**Figure 6.** (A) The unit cell content and (B) the packing arrangement of trigonal prisms for  $\alpha_{\text{L}}\text{-Ca}_2\text{SiO}_4$  polymorph is shown. (C) The unit cell content and (D) the packing arrangement of trigonal prisms for  $\alpha_{\text{H}}\text{-Ca}_2\text{SiO}_4$  polymorph structural model are shown. Si-O bonds are indicated with cyan lines. In (B,D), the structures are projected on the (010) planes, the trigonal prisms are demarcated with orange lines and the relative orientation of the ortho-hexagonal reference system is also indicated.

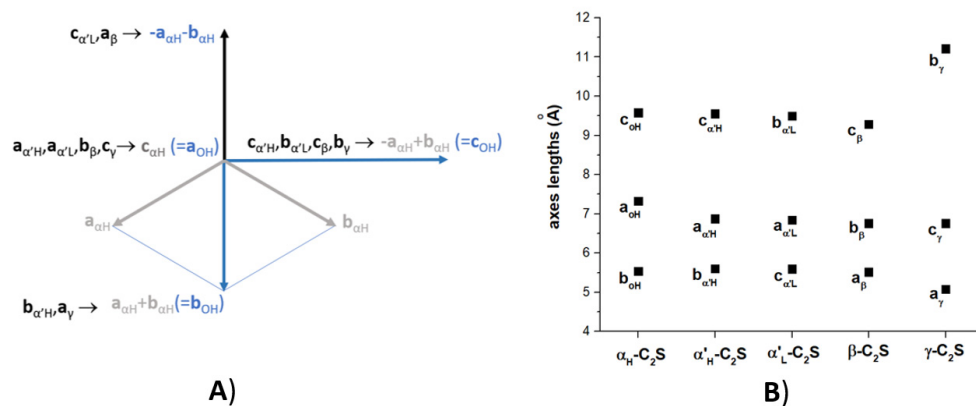


**Figure 7.** (A) The unit cell vector relations for the ortho-hexagonal axes ( $a_{\alpha'H}$ ,  $b_{\alpha'H}$ ,  $c_{\alpha'H} = -a_{\alpha'H} + b_{\alpha'H}$ ) with those of the hexagonal axes of  $\alpha_H$ -C<sub>2</sub>S polymorph ( $a_{\alpha'H}$ ,  $b_{\alpha'H}$  and  $c_{\alpha'H}$ ) are shown:  $a_{\alpha'H} = c_{\alpha'H}$ ,  $b_{\alpha'H} = a_{\alpha'H} + b_{\alpha'H}$  and  $c_{\alpha'H} = -a_{\alpha'H} + b_{\alpha'H}$ . The correspondence of the unit cell axes for the different polymorphs are also indicated. (B) Variation in unit cell values for all polymorphs of belite. The correspondences of the values for the axes of all the polymorphs with those of ortho-hexagonal cell of  $\alpha_H$ -C<sub>2</sub>S polymorph are given in Table 2.

Based on the original description in Barbier and Hyde [26], the basic building blocks for  $\beta$ - and  $\gamma$ -C<sub>2</sub>S polymorphs are the trigonal prisms of the Ca<sub>6</sub>Si type, shown in Figure 8. According to the previous discussion of the present work, these are also the building units of all the other belite polymorphs, resulting in the formation of “walls” consisting of edge-sharing columns of trigonal prisms. Adjacent walls are shifted along the stacking axis of the trigonal prisms, and this shift results in the capping of the slightly distorted orthorhombic faces of trigonal prisms belonging to one “wall” with Ca atoms belonging to neighboring “walls”. The number of capping Ca<sup>+2</sup> cations that lie at the equator plane is five. Figures S1–S6 give the detailed arrangement of calcium and silicon cations and also those of oxygen anions in the structure of all the polymorphs. In Figure 7, the arrangements of Ca<sup>+2</sup> cations around the Si<sup>+4</sup> one is presented with a coding name presentation but with direct correspondence with the detailed presentations of all the polymorphs in Figures S1–S6. Table S1 lists the different geometric parameters of all the trigonal prisms for all polymorphs. The average plane of the capped positions (B1, . . . , B5 sites in Figure 7) are shifted by half of the high of the trigonal prism in the  $\alpha$ -C<sub>2</sub>S trigonal/hexagonal (2.766/2.766 Å) and  $\alpha'_H$ -C<sub>2</sub>S (2.801/2.801 Å) cases of the  $\alpha$ -C<sub>2</sub>S trigonal/hexagonal (2.766/2.766) and  $\alpha'_H$ -C<sub>2</sub>S (2.801/2.801) and are approximately equal in the case of  $\gamma$ -C<sub>2</sub>S (2.548/2.534 Å). For  $\alpha'_L$ -C<sub>2</sub>S and for the prisms which host Si1 and Si2\*\*\* anions (Figure S4), the distances from the bases at the top (2.846 and 2.850 Å, respectively) are longer than those from the bottom of the prisms (2.737 and 2.738), and the opposite holds for the corresponding distances for the equator plane for the prism that hosts the Si3 anion (2.960/2.615). The average distances of Si from Ca cations which lie at both bases are equal, as is the distance from the corresponding planes of both trigonal bases in  $\alpha$ -C<sub>2</sub>S trigonal/hexagonal polymorphs (3.522/3.522 Å and 2.766/2.766 Å for trigonal 3.429/3.429 Å and 2.766/2.766 Å for the hexagonal model). Pairs of values with longer distances correspond to average distances of Si from Ca anions at the bases of trigonal prisms and the pairs of shorter ones correspond to distances to the base planes of the prisms. Both types of distances are equal in the case of  $\alpha'_H$ -C<sub>2</sub>S (3.533/3.533 Å and 2.801/2.801) and are approximately equal in the case of the  $\beta$ -C<sub>2</sub>S polymorph (3.472/3.485 and 2.756/2.736 Å). For  $\alpha'_L$ -C<sub>2</sub>S and for the prisms which host Si1 and S2\*\*\* anions (Figure S4), the distances of Si cations from the Ca ones that lie at the bottom are longer than those from the top, and the opposite holds for the corresponding distances for the Si3 anion in the respective prism. The same trend is observed for the corresponding distances of Si anions from the planes at the bottom and the top of the prisms (3.595/3.537 Å and 2.828/2.762 Å for S1; 3.649/3.407 Å and 2.985/2.576 Å for S2\*\*\*; 3.535/3.640 Å and 2.537/3.006 Å for S3, i.e., longer distances correspond to

average distances of Si from Ca anions at the bases of trigonal prisms). Although in the description given in [25] the number of anions on the equator plane is five, only the case of the  $\alpha$ -C<sub>2</sub>S trigonal/hexagonal polymorph seems to be satisfied based on the distances of Si cation from the Ca cations which occupy the B1, . . . , B5 sites. For trigonal polymorphs, the Si-B1, . . . , Si-B5 distances fall in the range of the values 3.198–3.782 Å, and those for hexagonal polymorphs in the range of 3.195–3.756 Å. In all the other cases, there are always two Ca cations that occupy sites at longer distances from the other three (Table S1). These are B3 and B5 (Si-B3: 4.226 Å and Si-B5: 3.778 Å) for  $\alpha'$ <sub>H</sub>-C<sub>2</sub>S; B2 and B4 for Si1 (Si1-B2: 3.728 and Si1-B4: 3.898 Å); B2 and B5 for Si2\*\*\* (Si2\*\*\*-B3: 4.167 and Si2\*\*\*-B5: 3.999 Å); B2 and B4 for Si3 (Si3-B3: 3.889 and Si3-B4: 4.340 Å) for  $\alpha'$ <sub>L</sub>-C<sub>2</sub>S; B2 and B4 (Si-B2: 3.812 and Si-B4: 4.009 Å) for  $\beta$ -C<sub>2</sub>S; and B3 and B4 (Si-B3: 4.834 and Si-B4: 4.834 Å) for  $\gamma$ -C<sub>2</sub>S. This result indicates that the nearest neighbors on the equator plane are five only for the high-temperature polymorphs (trigonal or hexagonal  $\alpha$ -C<sub>2</sub>S phase), and for the rest of the polymorphs the nearest neighbors are three, and thus the coordination polyhedron is a tricapped trigonal prism. Another factor that is important for the description of the structures of belite polymorphs is the sites that are occupied by the oxygen atoms. These are marked as T1, T2 and T3 and D2 and D3 in Figure 7. The T1, T2 and T3 sites are occupied in all polymorphs except  $\gamma$ -C<sub>2</sub>S (Figures S1–S6). The D1 sites are occupied in the case of  $\alpha$ -C<sub>2</sub>S trigonal polymorphs (Figure S1) and  $\alpha'$ <sub>H</sub>-C<sub>2</sub>S polymorphs (Figure S3) and D1 and D2 are occupied in the case of  $\alpha$ -C<sub>2</sub>S hexagonal polymorphs (Figure S2) and  $\alpha'$ <sub>H</sub>-C<sub>2</sub>S polymorphs (Figure S4). The oxygen atoms in the  $\gamma$ -C<sub>2</sub>S polymorph occupy unique sites that do not have a relationship with those occupied in the C<sub>2</sub>S polymorphs. In the same polymorph, the silicon polyhedron is a tricapped trigonal prism and the O1, O2, O3 and O3ii atoms occupy interstitial sites within the SiCa<sub>3</sub> tetrahedral type polyhedral, as presented in Figure S6 (Si1-Ca1\*-Ca1''-Ca2 for O1, Si1-Ca2\*\*'-Ca1-Ca1' for O2i, Si1-Ca2#-Ca1-Ca2' for O3 and Si1-Ca2\*\*\*-Ca1'-Ca2'' for O3ii; for symmetry codes, see Figure S6 caption). Another geometric parameter that has been discussed [26,36] as characterizing the relationship between the number of cupped positions and the dimensions of the trigonal prism is the ratio of the height (h of the prism) divided by the average length ( $\langle l \rangle$ ) of the triangular base edges. This parameter is  $h/\langle l \rangle = 1.507, 1.555, 1.554, 1.561, 1.582, 1.572$  and  $1.444$  for the  $\alpha$ -C<sub>2</sub>S trigonal/hexagonal,  $\alpha'$ <sub>H</sub>-C<sub>2</sub>S,  $\alpha'$ <sub>L</sub>-C<sub>2</sub>S(Si1),  $\alpha'$ <sub>L</sub>-C<sub>2</sub>S(Si2\*\*\*),  $\alpha'$ <sub>L</sub>-C<sub>2</sub>S(Si3),  $\beta$ -C<sub>2</sub>S and  $\gamma$ -C<sub>2</sub>S polymorphs, respectively, i.e., it increases upon transforming to a polymorph stabilized at lower temperature and takes the lowest value for the RT stabilized gamma polymorph. The similarities and characteristics of the different polymorphs of belite presented in this paragraph could support the general statement of Vegas in work [24], that cations in a structure could be considered as big molecules, and the anions act as an external factor such as pressure or temperature and thus could change their bonding patterns, which finally results in phase transformations. In addition, the present study supports the suggestion that the transformation mechanism, based on the relative disposition of cations for the different polymorphs, is of displacive character [26], but if we consider the sites occupied by oxygens at different polymorphs it could be considered as diffusion.

The present study could be of interest for the recent application of belite rare-earth doped compounds with the general formula  $\text{Ca}_{2-x}\text{Sr}_x\text{SiO}_4:\text{Ce}^{3+}$  [16], which present interesting luminescent properties. Depending on the Sr content, the compound crystallizes in the  $\beta$ - or  $\alpha'$ <sub>H</sub>-C<sub>2</sub>S polymorph. This result is consistent with the observation that the larger cations conform with an elongation of the height of trigonal prisms and thus to higher  $h/\langle l \rangle$  values [36]. According to the values given in Table S1, the highest values for the  $h/\langle l \rangle$  parameter are observed for the polymorphs  $\alpha'$ <sub>H</sub>-C<sub>2</sub>S,  $\alpha'$ <sub>L</sub>-C<sub>2</sub>S and  $\beta$ -C<sub>2</sub>S. The samples with composition  $\text{Ca}_{1.65}\text{Sr}_{0.25}\text{SiO}_4:0.10\text{Eu}^{2+}$  and  $\text{Ca}_{1.45}\text{Sr}_{0.35}\text{SiO}_4:0.10\text{Ce}^{3+}, 0.10\text{Li}^+$  crystallize in the  $\alpha'$ <sub>L</sub>-C<sub>2</sub>S polymorph [37]. Further study is needed in order to explore the factors that stabilize the different polymorphs of belite upon doping for luminescent applications, as systematic studies have revealed the formation of all five belite polymorphs [38]. The formation of all five polymorphs of belite at room temperature upon doping with different cations results in the synthesis of materials in two very active

research areas, i.e., belite-based cement products and photoluminescent ones. As these compounds are studied mostly in the form of polycrystalline materials, there is a need to have reliable powder diffraction diagrams in order to easily identify the most probable polymorph phases from the recorded diffraction pattern. Figure 9 presents all the simulated powder patterns of all five belite polymorphs which are discussed in the present work. For the calculations, the models obtained from the ICSD database which correspond to the entries listed in the Table 1 (or data from Table S2) were used, and they have been published in references [3,4]. Detailed structural models for all polymorphs are listed in Table S2. In Figure 9, the (hkl) indices for the main relaxions are also given. The indices of the hexagonal  $\alpha$ -C<sub>2</sub>S polymorph are given in gray color in the top pattern of Figure 9. In each pattern, the corresponding indices of the hexagonal system expressed with their values in the reference system of each polymorph are also given in gray color. The values for these indices are obtained by applying the relation  $(h'k'l') = (hkl)P$ , where  $P$  is the transformation matrix of the basis vectors for the related systems:  $(a',b',c') = (a,b,c)P$ . [39] The matrices used for all the transformations are listed in Table S3. No characteristic trend is observed concerning the presence of these reflections in the patterns of different polymorphs. In the patterns of all the polymorphs, additional peaks with low intensity are observed due to change in symmetry. The most characteristic observation concerns the peaks at around 32.5°, where splitting of intense peaks is observed in conformity with the experimental observations [38].

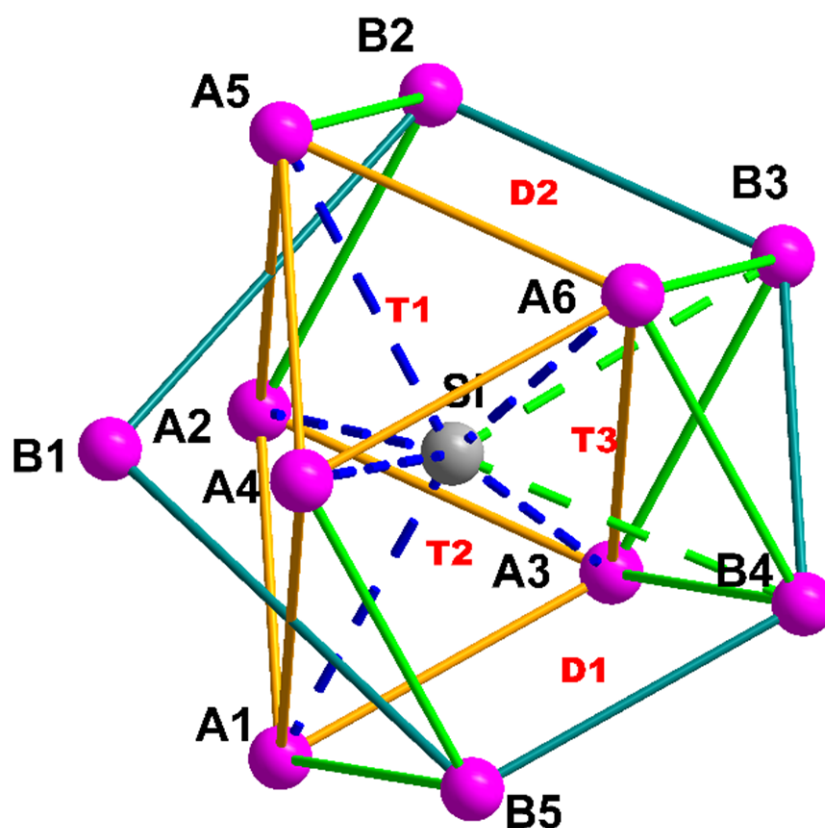


**Figure 8.** Arrangement of Ca cations around the Si<sup>+4</sup> cations in all belite polymorphs. A1, A2 and A3 indicate the Ca<sup>+2</sup> cations on the bottom trigonal face of the prism; A4, A5 and A6 indicate those at the top face of the prism; B1, . . . , B5 indicate those at the equator plane. T1, T2 and T3 and D1 and D2 indicate the sites of oxygen anions in different belite polymorphs.

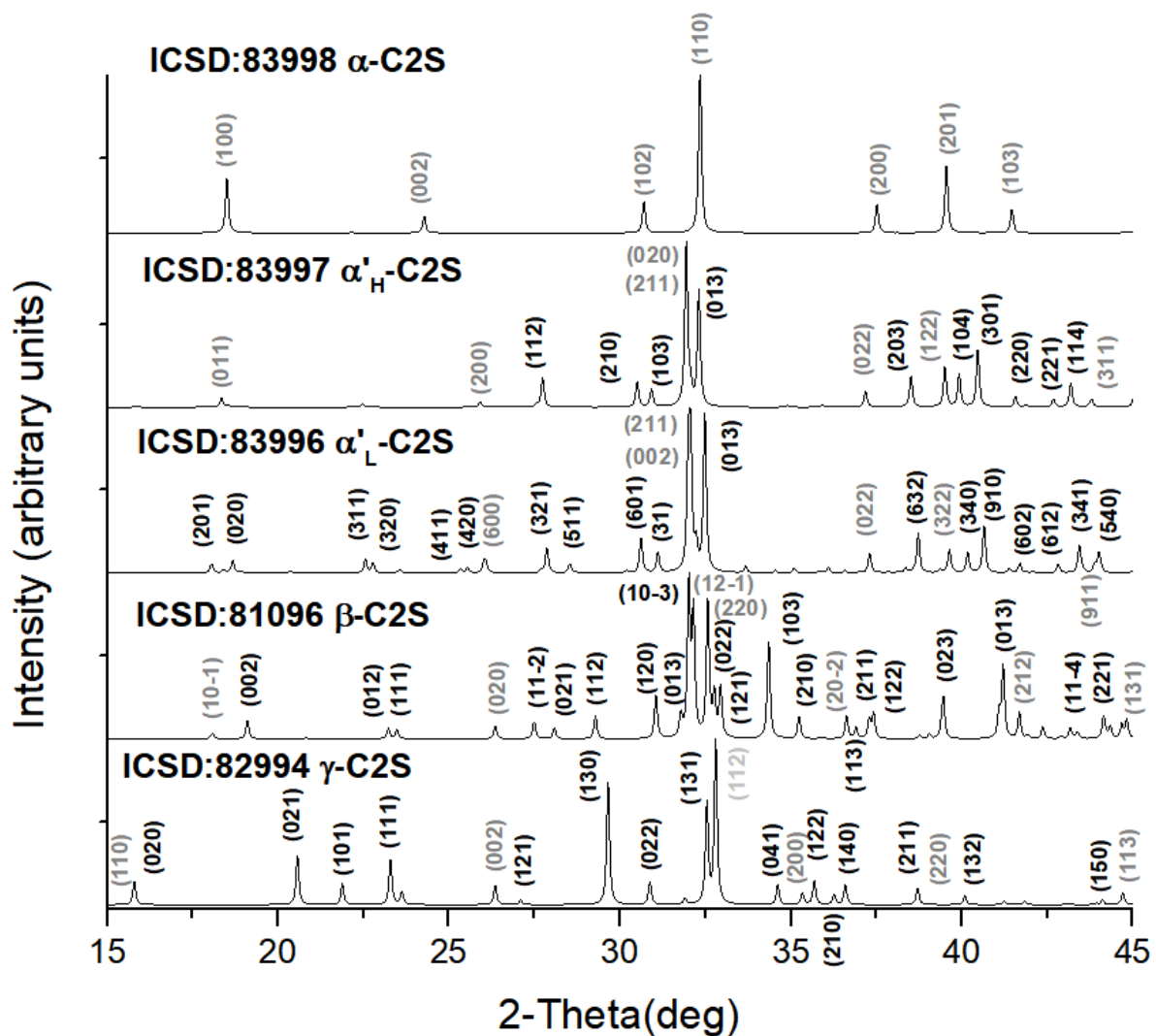


**Figure 9.** Simulated powder diffraction patterns for all the belite polymorphs (CuK $\alpha$  radiation) based on the ICSD data of the corresponding code numbers (Table 1 and Table S2).

#### 4. Conclusions

In the present study, the structure–superstructure relations of the five polymorphs of belite were derived based on unit cell axes relations. The common polyhedron of all polymorphs is a trigonal prism of calcium cations that hosts the silicon one, which is surrounded by five calcium cations at an equator plane for the  $\alpha$ -C2S trigonal/hexagonal polymorphs, thus forming a five-capped trigonal prism. For the rest of the polymorphs, the trigonal prisms are tri-capped ones, as three nearest neighbor calcium cations exist at the equator planes. In the  $\alpha$ -C2S to  $\gamma$ -C2S a significant increase is observed, normal in planes of the “walls” of trigonal prisms in addition to the usually mentioned volume increase. Based on the common characteristics of the arrangement of cations for all of the polymorphs, the transformation mechanism could be considered as displacive and, on the sites occupied by oxygen anions, could be considered of diffusion type. The systematic study of silicon dicalcium silicates could be not only for the cement industry but for the field of photoluminescent compounds.

**Supplementary Materials:** The following supporting information can be downloaded at: <https://www.mdpi.com/article/10.3390/cryst12121692/s1>, Figure S1: Presentation of the trigonal prism and the atoms at the equator plane for the  $\alpha$ -C<sub>2</sub>S trigonal polymorph; Figure S2: Presentation of the trigonal prism and the atoms at the equator plane for the  $\alpha$ -C<sub>2</sub>S hexagonal polymorph; Figure S3: Presentation of the trigonal prism and the atoms at the equator plane for the  $\alpha'$ H-C<sub>2</sub>S polymorph; Figure S4: Presentation of the trigonal prism and the atoms at the equator plane for the  $\alpha'$ L-C<sub>2</sub>S polymorph; Figure S5: Presentation of the trigonal prism and the atoms at the equator plane for the  $\beta$ -C<sub>2</sub>S trigonal polymorph; Figure S6: Presentation of the plane for the  $\gamma$ -C<sub>2</sub>S polymorph; Table S1: Geometric parameters of trigonal prisms; Table S2: trigonal prism and the atoms at the equator Crystallographic parameters for all studied structures.; Table S3: Transformation matrices of the unit cell axes which relate the cell axes of each belite polymorph with the hexagonal axes of the  $\alpha$ -C<sub>2</sub>S polymorph.

**Author Contributions:** Conceptualization, V.P. and M.C.; methodology, V.P., D.K. and M.C.; software, V.P. and M.C.; validation, V.P., M.C., D.K., M.K. and M.B.-K.; writing—original draft preparation, V.P.; writing—review and editing, V.P., M.C., D.K., M.K. and M.B.-K.; supervision, V.P., M.B.-K. and M.K.; project administration, V.P. and M.K. All authors have read and agreed to the published version of the manuscript.

**Funding:** This research was supported by NCSR “Demokritos” Industrial Research Fellowship Program (E.E.-12149) funded by the Stavros Niarchos Foundation and TITAN Cement S.A.

**Data Availability Statement:** Data available in a publicly accessible repository that does not issue DOIs. Publicly available datasets were analyzed in this study and the terms and conditions for accessing and using these data are given in the link: <https://www.ccdc.cam.ac.uk/access-structures-terms/>).

**Conflicts of Interest:** The authors declare no conflict of interest.

## References

1. Lawrence, C.D. The production of low-energy cements. In *Lea's Chemistry of Cement and Concrete*, 4th ed.; Butterworth-Heinemann: Oxford, UK, 2003.
2. Jost, K.H.; Ziemer, B.; Seydel, R. Redetermination of the structure of  $\beta$ -Dicalcium Silicate. *Acta Cryst.* **1977**, *B33*, 1696–1700. [[CrossRef](#)]
3. Mumme, W.G.; Hill, R.J.; Bushnell-Wye, G.; Segnit, E.R. Rietveld crystal structure refinements, crystal chemistry and calculated powder diffraction data for the polymorphs of dicalcium silicate and related phases. *Neues Jahrb. Fuer Mineral.—Abh.* **1995**, *169*, 35–68.
4. Mumme, W.G.; Cranswick, L.M.D.; Chakoumakos, B.C. Rietveld crystal structure refinements from high temperature neutron powder diffraction data for the polymorphs of dicalcium silicate. *Neues Jahrb. Fuer Mineral.—Abh.* **1996**, *170*, 171–188.
5. Mondal, P.; Jeffery, J.W. The Crystal Structure of Tricalcium Aluminate Ca<sub>3</sub>Al<sub>2</sub>O<sub>6</sub>\*. *Acta Cryst.* **1975**, *B31*, 689–697. [[CrossRef](#)]
6. Nishi, F.; Takeuchi, Y. The Al<sub>6</sub>O<sub>18</sub> Rings of tetrahedra in the structure of Ca<sub>8,5</sub>NaAl<sub>6</sub>O<sub>18</sub>. *Acta Cryst.* **1975**, *B31*, 1169–1173. [[CrossRef](#)]
7. Colville, A.A.; Geller, S. The crystal structure of brownmillerite, Ca<sub>2</sub>FeAlO<sub>5</sub>. *Acta Cryst.* **1971**, *B27*, 2311–2315. [[CrossRef](#)]
8. Colville, A.A.; Geller, S. Crystal structures of Ca<sub>2</sub>Fe<sub>1.43</sub>Al<sub>10.57</sub>O<sub>5</sub> and Ca<sub>2</sub>Fe<sub>1.28</sub>Al<sub>10.72</sub>O<sub>5</sub>. *Acta Cryst.* **1972**, *28*, 3196–3200. [[CrossRef](#)]
9. Dunstetter, F.; de Noirfontaine, M.-N.; Courtial, M. Polymorphism of tricalcium silicate, the major compound of Portland cement clinker: 1. Structural data: Review and unified analysis. *Cem. Concr. Res.* **2006**, *36*, 39–53. [[CrossRef](#)]
10. Yamnova, N.A.; Zubkova, N.V.; Eremin, N.N.; Zadov, A.E.; Gazeev, V.M. Crystal Structure of larnite  $\beta$ -Ca<sub>2</sub>SiO<sub>4</sub> and specific features of polymorphic transitions in dicalcium orthosilicate. *Struct. Inorg. Compd.* **2011**, *56*, 210–220. [[CrossRef](#)]
11. Courtial, M. Polymorphism of tricalcium silicate in Portland cement: A fast visual identification of structure and superstructure. *Powder Diffr.* **2012**, *18*, 7–15. [[CrossRef](#)]
12. de Noirfontaine, M.-N.; Dunstetter, F.; Courtial, M.; Gasecki, G.; Signes-Frehel, M. Tricalcium silicate Ca<sub>3</sub>SiO<sub>5</sub>, the major component of anhydrous Portland cement: On the conservation of distances and directions and their relationship to the structural elements. *Zeitschrift Fur Krist.* **2003**, *218*, 8–25. [[CrossRef](#)]
13. de Noirfontaine, M.-N.; Dunstetter, F.; Courtial, M.; Gasecki, G.; Signes-Frehel, M. Polymorphism of tricalcium silicate, the major compound of Portland cement clinker 2: Modelling alite for Rietveld analysis an industrial challenge. *Cem. Concr. Res.* **2006**, *36*, 54–64. [[CrossRef](#)]
14. de Noirfontaine, M.-N.; Dunstetter, F.; Courtial, M.; Gasecki, G.; Signes-Frehel, M. Tricalcium silicate Ca<sub>3</sub>SiO<sub>5</sub> superstructure analysis: A route towards the structure of the M1 polymorph. *Zeitschrift Fur Krist.* **2012**, *227*, 102–112. [[CrossRef](#)]
15. Manzano, H.; Durgun, E.; Qomi, M.J.A.; Ulm, F.J.; Pellenq, J.M.; Grossman, J.C. Impact of Chemical Impurities on the crystalline cement clinker phases determined by atomistic simulations. *Cryst. Growth Des.* **2011**, *11*, 2964–2972. [[CrossRef](#)]
16. Xia, Z.; Liu, Q. Progress in discovery and structural design of color conversion phosphors for LED. *Prog. Mater. Sci.* **2016**, *84*, 59–117. [[CrossRef](#)]
17. Chan, C.J.; Kriven, W.M.; Young, J.F. Physical Stabilization of the  $\beta \rightarrow \gamma$  Transformation in Dicalcium Silicate. *J. Am. Ceram. Soc.* **1992**, *75*, 1621–1627. [[CrossRef](#)]
18. Regourd, M.; Chromy, S.; Hjorth, L.; Mortureux, B.; Guinier, A. Polymorphisme des solutions solides du sodium dans l'aluminate tricalcique. *J. Appl. Crystallogr.* **1973**, *6*, 355–364. [[CrossRef](#)]

19. Ghosh, S.N.; Rao, P.B.; Paul, A.K.; Raina, K. The chemistry of dicalcium silicate mineral. *J. Mater. Sci.* **1979**, *14*, 1554–1566. [CrossRef]
20. Cuesta, A.; Lossilla, E.R.; Aranda, M.A.G.; De la Torre, A.G. Reactive belite stabilization mechanisms by boron-bearing dopands. *Cem. Concr. Res.* **2012**, *42*, 598–606. [CrossRef]
21. Moore, P.B.; Araki, T. The crystal structure of bredigite and the genealogy of some alkaline earth orthosilicates. *Am. Mineral.* **1976**, *61*, 74–87.
22. Pauling, L. *The Nature of the Chemical Bond and the Structure of Molecules and Crystals: An Introduction to Modern Structural Chemistry*, 3rd ed.; New York Cornell University Press: Ithaca, NY, USA, 1960; p. 505.
23. O’Keeffe, M.; Hyde, B.G. An Alternative Approach to Non-Molecular Crystal Structures with emphasis on the arrangements of cations. *Struct. Bond.* **1985**, *61*, 77–144.
24. Vegas, A. Cations in Inorganic Solids. *Crystallogr. Rev.* **2000**, *7*, 189–283. [CrossRef]
25. Vegas, A.; Mattesini, M. Towards a generalized vision of oxides: Disclosing the role of cations and anions in determining unit-cell dimensions. *Acta Cryst.* **2010**, *B66*, 338–344. [CrossRef] [PubMed]
26. Barbier, J.; Hyde, B.G. The Structures of the Polymorphs of Dicalcium Silicate,  $\text{Ca}_2\text{SiO}_4$ . *Acta Cryst.* **1985**, *B41*, 383–390. [CrossRef]
27. Butt, Y.M.; Timashev, V.V.; Malozohn, L.I. *Proceedings of the 5th International Symposium on the Chemistry of Cement*; Cement Association of Japan: Tokyo, Japan, 1968.
28. Koumpouri, D.; Angelopoulos, G.N. Effect of boron waste and boric acid addition on the production of low energy belite cement. *Cem. Concr. Comp.* **2016**, *68*, 1–8. [CrossRef]
29. Koumpouri, D.; Karatasios, I.; Psycharis, V.; Giannakopoylos, I.G.; Katsiotis, M.S.; Kilikoglou, V. Effect of clinkering conditions on phase evolution and microstructure of Belite Calcium-Sulpho-Aluminate cement clinker. *Cem. Concr. Res.* **2021**, *147*, 106529. [CrossRef]
30. DIAMOND—Crystal and Molecular Structure Visualization, Crystal Impact; Purts, H.; Brandenburg, K. (Eds.) GbR, Kreuzherrenstr: Bonn, Germany, 2009; Volume 102, p. 53227. Available online: <https://www.crystalimpact.de/diamond> (accessed on 2 October 2022).
31. Raman, R.S.K.; Gupta, R.K.; Sujir, M.N. Lattice constants of B8 structure in  $\text{Cu}_2\text{In-Ni}_2\text{In}$  alloys. *J. Sci. Res. Banaras Hindu Univ.* **1964**, *14*, 95–99.
32. Eckerlin, P.; Wölfel, E. Die Kristallstruktur von  $\text{Ca}_2\text{Si}$  und  $\text{Ca}_2\text{Ge}$ . *Z. Anorg. Allg. Chem.* **1955**, *280*, 321–331. [CrossRef]
33. Johson, V. Diffusionless Orthorhombic to Hexagonal Transitions in Ternary Silicides and Germanides. *Inorg. Chem.* **1975**, *14*, 1117–1120. [CrossRef]
34. Jeitscek, W. A High-Temperature X-ray Study of the Displacive Phase Transition in  $\text{MnCoGe}$ . *Acta Cryst.* **1975**, *B31*, 1187–1190. [CrossRef]
35. Kim, Y.J.; Nettleship, I.; Kriven, W.M. Phase Transformations in Dicalcium Silicate: II, TEM Studies of Crystallography, Microstructure, and Mechanisms. *J. Am. Ceram. Soc.* **1992**, *75*, 2407–2419. [CrossRef]
36. O’Keeffe, M.; Hyde, B.G. Some Structures Topologically Related to Cubic Perovskite ( $E2_1$ ),  $\text{ReO}_3$  ( $D0_9$ ) and  $\text{Cu}_3\text{Au}(L1_2)$ . *Acta Cryst.* **1977**, *B33*, 3802–3813. [CrossRef]
37. Xia, Z.; Miao, S.; Chen, M.; Molokeev, M.S.; Liu, Q. Structure, Crystallographic Sites, and Tunable Luminescence Properties of  $\text{Eu}^{2+}$  and  $\text{Ce}^{3+}/\text{Li}^+$ -Activated  $\text{Ca}_{1.65}\text{Sr}_{0.35}\text{SiO}_4$  Phosphors. *Inorg. Chem.* **2015**, *54*, 7684–7691. [CrossRef]
38. Mao, Z.; Lu, Z.; Chen, J.; Fahlman, B.D.; Wang, D. Tunable luminescent  $\text{Eu}^{2+}$ -doped dicalcium silicate polymorphs regulated by crystal engineering. *J. Mater. Chem. C* **2015**, *3*, 9454–9460. [CrossRef]
39. Arnold, H. Transformations of the coordinate system (unit-cell transformations). In *International Tables for Crystallography, Volume A, Space Group Symmetry*; Hahn, T., Ed.; Springer: Dordrecht, The Netherlands, 2005; Chapter 5; p. 77.